

EUROPHYSICS LETTERS

Europhys. Lett., (), pp. ()

Burst dynamics during drainage displacements in porous media: Simulations and experiments

EYVIND AKER^{1,2}, KNUT JØRGEN MÅLØY¹, ALEX HANSEN² AND SOUMEN BASAK³¹ *Department of Physics, University of Oslo, N-0316 Oslo, Norway*² *Department of Physics, Norwegian University of Science and Technology, N-7491 Trondheim, Norway*³ *Saha Institute of Nuclear Physics, 1/AF Bidhannagar, Calcutta 700064, India*

(received ; accepted)

PACS. 47.55Mh – Flows through porous media.

PACS. 47.55Kf – Multi-phase and particle-laden flows.

PACS. 05.40–a – Fluctuation phenomena, random processes, noise, and Brownian motion.

PACS. 07.05Tp – Computer modeling and simulation.

Abstract. – We investigate the burst dynamics during drainage going from low to high injection rate at various fluid viscosities. The bursts are identified as pressure drops in the pressure signal across the system. We find that the statistical distribution of pressure drops scales according to other systems exhibiting self-organized criticality. The pressure signal was calculated by a network model that properly simulates drainage displacements. We compare our results with corresponding experiments.

Since the early 1980s physicists have paid attention to the complex phenomena observed when one fluid displaces another fluid in porous media. The papers that have appeared in the literature mostly refer to the rich variety of displacement structures that is observed due to different fluid properties like flow rate, viscosity, interfacial tension, and wettability. The major displacement structures have been found to resemble structures generated by geometrical models like invasion percolation (IP) [1, 2, 3], DLA [4, 5, 6, 7], and anti-DLA [5, 8]. Only a few authors [9, 10, 11] have addressed the interplay between the displacement structures and the evolution of the fluid pressure. In slow drainage when non-wetting fluid displaces slowly wetting fluid in porous media, the pressure evolves according to Haines jumps [9, 12, 13]. The displacement is controlled solely by the pressure difference between the two fluids across a meniscus (the capillary pressure), and the non-wetting fluid invades the porous medium in a series of bursts accompanied by sudden negative pressure drops.

The purpose of this paper is to study the dynamics of the fluid pressure during drainage going from low to high displacement rates. To do so, we examine the statistical properties of the sudden negative pressure drops due to the bursts. We find that for a wide range of displacement rates and fluid viscosities, the pressure drops act in analogy to theoretical predictions of systems exhibiting self-organized criticality [14], like IP. Even at high injection rates, where

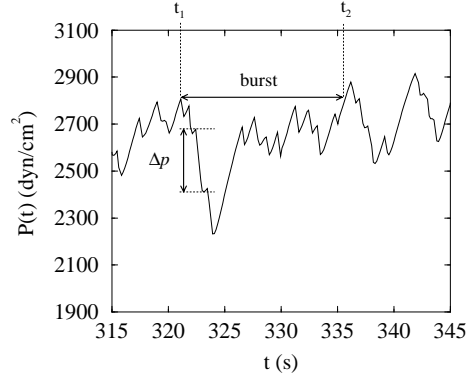


Fig. 1. – The pressure signal as function of injection time, $P(t)$, for one simulation at low displacement rate in a narrow time interval. The horizontal line defines the pressure valley of a burst that last a time period $T = t_2 - t_1$. Note that the valley may contain a hierarchical structure of smaller valleys inside. The vertical line indicates the size of a local pressure jump Δp inside the valley.

the connection between the displacement process and IP is more open, the pressure drops behave similar to the case of extreme low injection rate, where IP apply. The pressures are calculated by a network model that properly simulates the fluid-fluid displacement. Moreover, we measure the fluid pressure in drainage experiments and compare that with our simulation results.

In the simulations a burst starts where the pressure drops suddenly and stops where the pressure has raised to a value above the pressure that initiated the burst (see fig. 1). Thus, a burst may consist of a large pressure valley containing a hierarchical structure of smaller pressure jumps (*i.e.* bursts) inside. A pressure jump, indicated as Δp in fig. 1, is the pressure difference from the point where the pressure starts decreasing minus the pressure where it stops decreasing. We define the size of the pressure valley (valley size) to be $\chi \equiv \sum_i \Delta p_i$, where the summation index i runs over all the pressure jumps Δp_i inside the valley. The definition is motivated by experimental work in ref. [13]. For slow displacements we have that χ is proportional to the geometric burst size s , being invaded during the pressure valley. This statement has been justified in ref. [13], where it was observed that in stable periods, the pressure increased linearly as function of the volume being injected into the system. Later, in an unstable period where the pressure drops abruptly due to a burst, this volume is proportional to s . At fast displacements the pressure may no longer be a linear function of the volume injected into the system. Therefore, a better estimate of s there, is to compute the time period T of the pressure valley (fig. 1). Since the displacements are performed with constant rate, it is reasonable to assume that T is always proportional to the volume being injected during the valley and hence, $T \propto s$.

We have computed the distributions of χ and T from the pressure signals of simulations and experiments. We find that the distributions are consistent with a power law, independent of injection rate and fluid viscosities (figs. 2 and 4) and that the distribution of pressure jumps Δp_i , follows an exponential decreasing function (fig. 3).

The network model used in the simulations is thoroughly discussed in refs. [15] and [16] and only its main features are presented below. The porous medium consists of a two-dimensional

(2D) square lattice of cylindrical tubes oriented at 45° relative to one of the edges of the lattice. Four tubes meet at each intersection where we put a node having no volume. The disorder is introduced by moving the intersections a randomly chosen distance away from their initial positions, giving a distorted square lattice. The distances are chosen in the interval between zero and less than one half of the grid size to avoid overlapping intersections in the new lattice. We let d_{ij} denote the length of the tube between node (intersection) i and j in the lattice and $r_{ij} = d_{ij}/2\alpha$ defines the corresponding radius of the tube. Here α is the aspect ratio between the tube length and its radius.

The tubes are initially filled with a wetting fluid of viscosity μ_w , and a non-wetting fluid of viscosity μ_{nw} is injected at constant injection rate Q along the bottom row. The wetting fluid is displaced and flows out along the top row and there are periodic boundary conditions in the horizontal direction. The fluids are assumed incompressible and immiscible and an interface (meniscus) is located where the fluids meet in the tubes. The capillary pressures of the menisci behave as if the tubes were hourglass shaped with effective radii following a smooth function. Thus, we let the capillary pressure p_c be a function of the meniscus' position in the tube in the following way: $p_c = (2\gamma/r)[1 - \cos(2\pi x/d)]$. Here we have omitted the subscripts ij . The first term results from Young-Laplace law when assuming that the principal radii of curvature of the meniscus are equal to the radius of the tube, and that the wetting fluid perfectly wets the medium. γ denotes the interfacial tension between the fluids. In the second term x is the position of the meniscus in the tube, *i.e.* $0 \leq x \leq d$. The advantage of the above approach is that we include the effect of local readjustments of the menisci on pore level [15], which is important for the description of the burst dynamics [9, 13].

The fluid flow q_{ij} through a tube from node i to node j , is solved by using Hagen-Poiseuille flow in cylindrical tubes and Washburn's approximation [17] for menisci under motion giving, $q_{ij} = -(\sigma_{ij}k_{ij}/\mu_{ij})(p_j - p_i - p_{c,ij})/d_{ij}$. Here p_i and p_j are the pressures at the nodes, $p_{c,ij}$ is the capillary pressure if one or two menisci are present in the tube, and μ_{ij} is the effective viscosity of the fluids occupying the tube. k_{ij} and σ_{ij} is the permeability and the cross section of the tube, respectively. By inserting the above equation into Kirchhoff equations at every node, $\sum_j q_{ij} = 0$, constitutes a set of linear equations which are solved for the nodal pressures p_i . The set of linear equations is solved by the Conjugate Gradient method [18]. See refs. [15] and [16] for how the menisci are updated and other numerical details about the network model.

To characterize the fluid properties used in the simulations, we use the capillary number C_a and the viscosity ratio M . C_a , denoting the ratio of capillary and viscous forces, is in the following defined as $C_a \equiv Q\mu/\Sigma\gamma$. Here μ is maximum viscosity of μ_{nw} and μ_w , and Σ is the cross section of the inlet. The viscosity ratio M , is defined as $M \equiv \mu_{nw}/\mu_w$.

We have performed three different series of simulations with $M = 0.01, 1, \text{ and } 100$, respectively. In each series C_a was varied by adjusting the injection rate Q . To obtain reliable average quantities we did 10 to 20 simulations of different distorted lattices, at each C_a . The lattice size of the networks was 60×90 nodes for $M = 0.01$, 40×60 nodes for $M = 1$, and 25×35 nodes for $M = 100$. In all simulations we set $\gamma = 30$ dyn/cm, and the radii of the tubes were inside the interval $[0.08, 0.72]$ mm. The average tube length was always 1 mm. The parameters were chosen to be close to the experimental setup in [9].

For all simulations we calculated the hierarchical valley size distribution $N_{\text{all}}(\chi)$. The distribution was calculated by including all valley sizes and the hierarchical smaller ones within a large valley (see fig. 1). The result for high, intermediate, and low C_a when $M = 1$ and $M = 100$ is shown in a logarithmic plot in fig. 2. Identical results were obtained for $M = 0.01$. In order to calculate the valley sizes at large C_a , we subtract the average drift in the pressure signal due to viscous forces such that the pressure becomes a function that fluctuates around some mean pressure.

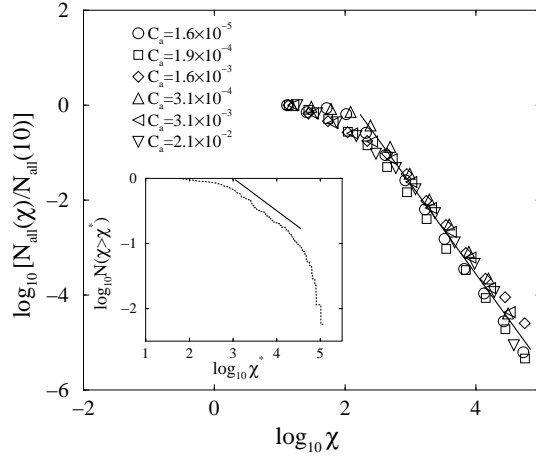


Fig. 2. – The hierarchical valley size distribution $N_{\text{all}}(\chi)$, for simulations between low and high C_a with $M = 1$ (\circ, \square, \diamond) and $M = 100$ ($\triangle, \triangleleft, \nabla$). The slope of the solid line is -1.9 . *Inset*: The cumulative valley size distribution $N(\chi > \chi^*)$, for bursts that start in a narrow pressure strip for the simulation performed at $C_a = 1.6 \times 10^{-5}$. The slope of the solid line is -0.5 .

By assuming a power law $N_{\text{all}}(\chi) \propto \chi^{-\tau_{\text{all}}}$ our best estimate from fig. 2 is $\tau_{\text{all}} = 1.9 \pm 0.1$, indicated by the slope of the solid line. At low χ in fig. 2, typically only one tube is invaded during the valley and we do not expect the power law to be valid. Similar results were obtained when calculating the hierarchical distribution of the time periods T of the valleys, denoted as $N_{\text{all}}(T)$.

In IP the distribution of burst sizes $N(s)$, where s denotes the burst size, is found to obey the scaling relation [9, 13, 19, 20]

$$N(s) \propto s^{-\tau'} g(s^\sigma (f_0 - f_c)). \quad (1)$$

Here f_c is the percolation threshold of the system and $g(x)$ is some scaling function, which decays exponentially when $x \gg 1$ and is a constant when $x \rightarrow 0$. τ' is related to percolation exponents like $\tau' = 1 + D_f/D - 1/(D\nu)$ [20], where D_f and D is the fractal dimension of the front and the mass of the percolation cluster, respectively. D_f depends on the definition of the front, that is, D_f equals D_e for external perimeter growth zone [21, 22] and D_h for hull perimeter growth zone [22, 23]. ν is the correlation length exponent in percolation theory and $\sigma = 1/(\nu D)$ [22]. In eq. (1) a burst is defined as the connected structure of sites that is invaded following one root site of random number f_0 , along the invasion front. All sites in the burst have random numbers smaller than f_0 , and the burst stops when $f > f_0$, is the random number of the next site to be invaded [24].

By integrating eq. (1) over all f_0 in the interval $[0, f_c]$ Maslov [14] deduced a scaling relation for the hierarchical burst size distribution $N_{\text{all}}(s)$ following

$$N_{\text{all}}(s) \propto s^{-\tau_{\text{all}}}, \quad (2)$$

where $\tau_{\text{all}} = 2$.

In the low C_a regime in fig. 2, the displacements are in the capillary dominated regime and the invading fluid generates a growing cluster similar to IP [1, 2, 25, 26]. In this regime we also

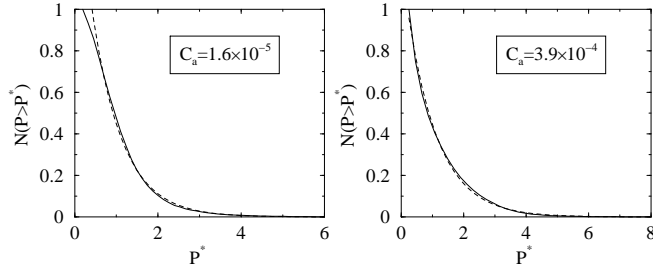


Fig. 3. – The cumulative pressure jump distribution function $N(P > P^*)$, for simulations performed with viscosity matched fluids ($M = 1$). The dashed lines are fitted exponential functions.

have that $\chi \propto s$ [13] and hence $N_{\text{all}}(\chi)$ corresponds to $N_{\text{all}}(s)$ in eq. (2). Thus, in the low C_a regime we expect that $N_{\text{all}}(\chi)$ follows a power law with exponent $\tau_{\text{all}} = 2$ which is confirmed by our numerical results. Similar results were obtained in ref. [13].

The evidence in fig. 2, that τ_{all} does not seem to depend on C_a , is very interesting and new. At high C_a when $M = 0.01$ an unstable viscous fingering structure generates and when $M \geq 1$ a stable front develops. It is an open question how these displacement processes map to the proposed scaling in eq. (2). We note that in the high C_a regime the relation $\chi \propto s$ may not be correct and T is preferred when computing N_{all} . However, the simulations show that $N_{\text{all}}(\chi) \sim N_{\text{all}}(T)$ even at high C_a .

In [14] it was pointed out that τ_{all} is super universal for a broad class of self-organized critical models including IP. Our result in fig. 2 indicates that the simulated displacement processes might belong to the same super universality class even at high injection rates.

Maslov [14] also calculated the time-reversed (backward) hierarchical burst size distribution and predicted that this distribution should follow a power law with a model-dependent exponent τ_{all}^b . In our case we are dealing with 2D IP with trapping giving $\tau_{\text{all}}^b = 1.68$. We have calculated τ_{all}^b of our simulations by simply reversing the time axis in the pressure signal in fig. 1 and repeating the steps which led to fig. 2. From that we obtain $\tau_{\text{all}}^b = 1.7 \pm 0.1$ which is consistent with the predictions in [14].

In the inset of fig. 2 we have plotted the cumulative valley size distribution $N(\chi > \chi^*)$ for the simulation at lowest $C_a = 1.6 \times 10^{-5}$ with $M = 1$. $N(\chi > \chi^*)$ was calculated for bursts that starts at pressures in a narrow strip between 2800 and 3100 dyn/cm² where 3100 is the maximum pressure during the displacement. From eq. (1) we have that $N(s) \propto s^{-\tau'}$ for bursts that start close to the percolation threshold f_c . In our simulations f_c corresponds to the maximum pressure. It is hard to observe any power law in the inset of fig. 2, however, if we assume one, our best estimate is $1 - \tau' = -0.5$ as indicated by the slope of the solid line. In [13] simulations and experiments gave $1 - \tau' = -0.45 \pm 0.10$. We need larger system sizes and more simulations to improve our statistics, but we conclude that our result are in agreement of [13].

We have also calculated the cumulative pressure jump distribution function $N(P > P^*)$ for the simulations with $M = 1$ and 100 at various injection rates. Here $P \equiv \Delta p / \langle \Delta p \rangle$ where $\langle \Delta p \rangle$ is the mean of the local pressure jumps Δp in the pressure signal (see fig. 1). The result for two simulation, one at high and the other at low C_a , is plotted in fig. 3. Both were performed with viscosity matched fluids ($M = 1$). The distributions have been fitted to exponentially decreasing functions drawn as dashed lines in fig. 3. At low C_a we find

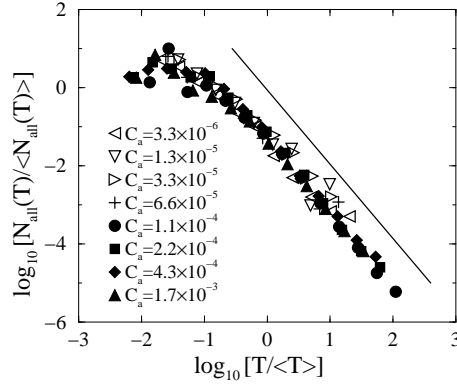


Fig. 4. – The hierarchical distribution $N_{\text{all}}(T)$ of the valley time T during a burst, for experiments (open symbols) and simulations (filled symbols) at various C_a with $M = 0.017$ and $M = 0.01$, respectively. The slope of the solid line is -1.9 .

$N(P > P^*) \propto e^{-1.38P^*}$, which is consistent with results in [13]. At high C_a the distribution function was fitted to $e^{-1.02P^*}$. The pre-factor in the exponent of the exponential function seems to change systematically from about 1.4 to 1.0 as C_a increases. Similar results were obtained from simulations performed with $M = 100$.

We have performed four drainage experiments where we used a 110×180 mm transparent porous model consisting of a mono-layer of randomly placed glass beads of 1 mm, sandwiched between two Plexiglas plates [9]. The model was initially filled with a water-glycerol mixture of viscosity 0.17 P. The water-glycerol mixture was withdrawn from one of the short side of the system at constant rate by letting air enter the system from the other short side. The pressure in the water-glycerol mixture on the withdrawn side was measured with a pressure sensor of our own construction.

From the recorded pressure signal we calculated the hierarchical distribution of time periods of the valleys, $N_{\text{all}}(T)$. At low C_a this corresponds to $N_{\text{all}}(s)$ in eq. (2). Because of the relative long response time of the pressure sensor, rapid and small pressure jumps due to small bursts are presumably smeared out by the sensor and the recorded pressure jumps are only reliable for larger bursts. Hence, from the recorded pressure signal T appears to be a better estimate of the burst sizes than χ .

In fig. 4 we have plotted the logarithm of $N_{\text{all}}(T)$ for experiments (open symbols) and simulations (filled symbols) performed at four different C_a , respectively. To collapse the data $N_{\text{all}}(T)$ and T were normalized by their means. In the simulations $M = 0.01$ while in the experiments $M = 0.017$ where we have assumed air to have viscosity 0.29×10^{-2} P. We observe that the experimental result is consistent with our simulations and we conclude that $N_{\text{all}}(T) \propto T^{1.9 \pm 0.1}$. This confirms the scaling of $N_{\text{all}}(\chi)$ in fig. 2. We have also calculated the time-reversed distribution of $N_{\text{all}}(T)$ and the result of that is consistent with the time-reversed distribution that was calculated of the simulations in fig. 2.

Note that when comparing the C_a 's of the experiments with the ones of the simulations in fig. 4, we have to take into account the different system sizes. The length of the experimental setup is about three times larger than the length of the simulation network. Therefore we expect that in the experiments, viscous fingering develops at C_a 's of about three times less

than in the simulations.

In summary we find that $\tau_{\text{all}} = 1.9 \pm 0.1$ for all displacement simulations going from low to high injection rates when $M = 0.01, 1, \text{ and } 100$. This is also confirmed by drainage experiments performed at various injection rates with $M = 0.017$. At low injection rates the result is consistent with the prediction in [14] ($\tau_{\text{all}} = 2$), which was deduced for a broad spectrum of different self-organized critical models including IP. The evidence that τ_{all} is independent of the injection rate, may indicate that the displacement process belongs to the same super universality class as the self-organized critical models in [14], even where there is no mapping between the displacement process and IP. The good correspondence between our simulation results and the drainage experiments in fig. 4 and also the results reported at slow drainage in [13], demonstrates that the burst dynamics is well described by our simulation model.

The authors thank S. Roux for valuable comments. The work is supported by the Norwegian Research Council (NFR) through a ‘‘SUP’’ program and we acknowledge them for a grant of computer time.

REFERENCES

- [1] WILKINSON D. and WILLEMSSEN J. F., *J. Phys. A*, **16** (1983) 3365.
- [2] LENORMAND R. and ZARCONE C., *Phys. Rev. Lett.*, **54** (1985) 2226.
- [3] CIEPLAK M. and ROBBINS M. O., *Phys. Rev. Lett.*, **60** (1988) 2042.
- [4] WITTEN T. A. and SANDER L. M., *Phys. Rev. Lett.*, **47** (1981) 1400.
- [5] L. PATERSON, *Phys. Rev. Lett.*, **52** (1984) 1621.
- [6] CHEN J.-D. and WILKINSON D., *Phys. Rev. Lett.*, **55** (1985) 1892.
- [7] MÅLØY K. J., FEDER J. and JØSSANG T., *Phys. Rev. Lett.*, **55** (1985) 26881.
- [8] LENORMAND R., TOUBOUL E. and ZARCONE C., *J. Fluid Mech.*, **189** (1988) 165.
- [9] MÅLØY K. J., FURUBERG L., FEDER J. and JØSSANG T., *Phys. Rev. Lett.*, **68** (1992) 2161.
- [10] VAN DER MARCK S.C., MATSUURA T. and GLAS J., *Phys. Rev. E*, **56** (1997) 5675.
- [11] VAN DER MARCK S. C. and GLAS J., *Eur. J. Mech., B/Fluids*, **16** (1997) 681.
- [12] W. B. HAINES, *J. Agr. Sci.*, **20** (1930) 97.
- [13] FURUBERG L., MÅLØY K. J. and FEDER J., *Phys. Rev. E*, **53** (1996) 966.
- [14] S. MASLOV, *Phys. Rev. Lett.*, **74** (1995) 562.
- [15] AKER E., MÅLØY K. J., HANSEN A. and BATROUNI G. G., *Transp. Porous Media*, **32** (1998) 163.
- [16] AKER E., MÅLØY K. J. and HANSEN A., *Phys. Rev. E*, **58** (1998) 2217.
- [17] E. W. WASHBURN, *Phys. Rev.*, **17** (1921) 273.
- [18] BATROUNI G.G. and HANSEN A., *J. Stat. Phys.*, **52** (1988) 747.
- [19] SAPOVAL B., ROSSO M., and GOUYET J. F., in *Fractals' Physical Origin and Properties*, edited by L. PIETRONERO, (Plenum Press, New York) 1989.
- [20] MARTYS N., ROBBINS M. O. and CIEPLAK M., *Phys. Rev. B.*, **44** (1991) 12294.
- [21] GROSSMAN T. and AHARONY A., *J. Phys. A: Math. Gen.*, **20** (1987) L1193.
- [22] STAUFFER D. and AHARONY A., *Introduction to percolation theory*, (Taylor & Francis, London, Great Britain) 1992.
- [23] R. F. VOSS, *J. Phys. A: Math. Gen.*, **17** (1984) L373.
- [24] ROUX S. and GUYON E., *J. Phys. A: Math. Gen.*, **22** (1989) 3693.
- [25] DE GENNES P.G. and GUYON E., *J. Mec. (Paris)*, **17** (1978) 403.
- [26] CHANDLER R., KOPLIK J., LERMAN K. and WILLEMSSEN J. F., *J. Fluid Mech.*, **119** (1982) 249.